Keratin 9 Is Required for the Structural Integrity and Terminal Differentiation of the Palmoplantar Epidermis

Dun Jack Fu[1], Calum Thomson[2], Declan P. Lunny[3], Patricia J. Dopping-Hepenstal[4], John A. McGrath[5], Frances J.D. Smith[1], W.H. Irwin McLean[1] and Deena M. Leslie Pedrioli[1]

Keratin 9 (K9) is a type I intermediate filament protein whose expression is confined to the suprabasal layers of the palmoplantar epidermis. Although mutations in the K9 gene are known to cause epidermolytic palmoplantar keratoderma, a rare dominant-negative skin disorder, its functional significance is poorly understood. To gain insight into the physical requirement and importance of K9, we generated K9-deficient (*Krt9*$^{-/-}$) mice. Here, we report that adult *Krt9*$^{-/-}$ mice develop calluses marked by hyperpigmentation that are exclusively localized to the stress-bearing footpads. Histological, immunohistochemical, and immunoblot analyses of these regions revealed hyperproliferation, impaired terminal differentiation, and abnormal expression of keratins K5, K14, and K2. Furthermore, the absence of K9 induces the stress-activated keratins K6 and K16. Importantly, mice heterozygous for the K9-null allele (*Krt9*$^{+/-}$) show neither an overt nor histological phenotype, demonstrating that one *Krt9* allele is sufficient for the developing normal palmoplantar epidermis. Together, our data demonstrate that complete ablation of K9 is not tolerable *in vivo* and that K9 is required for terminal differentiation and maintaining the mechanical integrity of palmoplantar epidermis.

INTRODUCTION

Keratin 9 (K9; gene name *KRT9* in humans; *Krt9* in mice), is a type I intermediate filament protein specifically expressed in the suprabasal layers of the primary epidermal ridges of the palmoplantar epidermis in humans (Knapp *et al.*, 1986; Swensson *et al.*, 1998). In adult mice, *Krt9* is expressed in the footpads, which is equivalent to human thick skin (Schweizer *et al.*, 1989). In both humans and mice, the palmoplantar epidermis must withstand the highest degree of mechanical stress the body is exposed to and is, therefore, a highly specialized tissue abundantly expressing a diverse set of keratins. The site and tissue-specific expression pattern of *Krt9* in glabrous epidermis has been postulated to provide additional mechanical reinforcement by promoting filament bundling (Schweizer *et al.*, 1989; Swensson *et al.*, 1998). Nevertheless, the functional importance

and specific requirement for K9, as well as other individual keratins, within the palmoplantar epidermis remains unclear.

Epidermolytic palmoplantar keratoderma (EPPK) is one of >30 rare autosomal-dominant human keratinizing disorders characterized by diffuse hyperkeratosis on the palms and soles (Omary *et al.*, 2004; McLean and Irvine, 2007; McLean and Moore, 2011; Haines and Lane, 2012). EPPK is unique among the keratinopathies, in that it is exclusively caused by dominant-negative mutations in *KRT9* (Smith, 2003; McLean and Irvine, 2007). This pathomechanism makes EPPK well suited for the development of RNA interference-based therapeutics that specifically inhibits the activity of the causative keratin allele. The monogenic nature of EPPK; the hotspot mutations in *KRT9* that account for the majority of all EPPK cases; the well-circumscribed and accessible treatment area; and the abundance of other keratins in the palmoplantar epidermis, all combine to make this a good model disease for therapeutic small interfering RNA (siRNA) proof-of-concept studies. To this end, we recently developed a RNA interference-based therapeutic package for EPPK with mutation-specific siRNAs that inhibit four of the most common *KRT9* mutations (Leslie Pedrioli *et al.*, 2012). No recessive or loss-of-function mutations have been reported for *KRT9* and functional redundancy has been shown for other palmoplantar keratins (Porter and Lane, 2003; Coulombe *et al.*, 2004; Lu *et al.*, 2006). It, therefore, also stands to reason that complete inhibition of *KRT9* might be a viable therapy strategy for EPPK. To investigate this, potent generic siRNAs that target *KRT9* regardless of the EPPK mutation status were also developed (Leslie Pedrioli *et al.*, 2012).

[1]*Division of Molecular Medicine and Centre for Dermatology and Genetic Medicine, Colleges of Life Sciences and Medicine, Dentistry and Nursing, University of Dundee, Dundee, UK;* [2]*Microscopy Facility, College of Life Sciences, University of Dundee, Dundee, UK;* [3]*Epithelial Biology Group, Institute of Medical Biology, Immunos, Singapore;* [4]*Guy's and St Thomas' (GSTS) Pathology, St Thomas' Hospital, London, UK and* [5]*St John's Institute of Dermatology, King's College London, London, UK*

Correspondence: Deena M. Leslie Pedrioli, Division of Molecular Medicine and Centre for Dermatology and Genetic Medicine, College of Life Sciences and Medicine, Dentistry and Nursing, University of Dundee, Dundee DD1 5EH, UK. E-mail: d.lesliepedrioli@dundee.ac.uk

Although our proof-of-principle studies demonstrated specificity and potency of K9 siRNAs both *in vitro* and *in vivo*, we were unable to assess their efficacy, tolerance, or potential therapeutic benefits under endogenous conditions (Leslie Pedrioli *et al.*, 2012). Furthermore, a recent study demonstrating that K16-null mice develop a phenotype closely resembling palmoplantar keratoderma (Lessard and Coulombe, 2012) strongly suggested that keratin functional redundancy within the palmoplantar epidermis may not be as extensive as originally thought. To determine whether complete ablation of K9 *in vivo* could be a viable therapeutic option for EPPK patients and define the functional importance of this palmoplantar keratin *in vivo*, we generated gene-targeted mice deficient for *Krt9*.

RESULTS

K9-deficient (*Krt9*$^{-/-}$) mice develop hyperpigmented calluses on their stress-bearing footpads

Krt9-null mice were generated using *Krt9*-null C57 Bl/6NTac ES cells obtained from the Knock-Out Mouse Project repository (Supplementary Figure S1a online; see Supplementary Information online). *Krt9*$^{+/+}$, *Krt9*$^{+/-}$, and *Krt9*$^{-/-}$ mice were born at approximate Mendelian ratios. Appropriate expression of *Krt9* and *lacZ* within the suprabasal layers of palmoplantar epidermis (Knapp *et al.*, 1986; Schweizer *et al.*, 1989; Swensson *et al.*, 1998) of *Krt9*$^{+/+}$, *Krt9*$^{+/-}$, and *Krt9*$^{-/-}$ littermates was confirmed via western blotting and immunohistochemical staining (Supplementary Figure S1b and S1c online; see Supplementary Information online).

Initially, newborn *Krt9*$^{+/-}$ and *Krt9*$^{-/-}$ mice were visually indistinguishable from *Krt9*$^{+/+}$ littermates. Surprisingly, hyperpigmented calluses began to develop on the rear, stress-bearing fore-paw footpads of *Krt9*$^{-/-}$ animals between 3 and 4 weeks of age, which persisted into adulthood (Figure 1a). We monitored the progression of this phenotype at weekly intervals in adult mice and found that the presence, severity and pigmentation state of these calluses cycled over the 8-week study period (Figure 1b). Indeed, every 3 weeks we observed hyperpigmentation intensify and callus size increase and then, just prior to the callus sloughing-off, localized flakiness would develop on the calluses. This phenotype was most evident on the major footpads of the fore-paws, but it was also observed to a lesser extent on the minor footpads of both the fore- and hind-paws of these animals (Figure 1b; and data not shown). Importantly, neither the presence nor state of the callus appeared to affect animal mobility or their ability to thrive. This phenotype was not observed in *Krt9*$^{+/+}$ and *Krt9*$^{+/-}$ littermates (Figure 1a; and data not shown).

K9-null mouse fore- and hind-paw footpads develop localized acanthosis and hyperkeratosis

Histological analysis of the fore- and hind-paw footpads of 8-week old *Krt9*$^{+/+}$, *Krt9*$^{+/-}$, and *Krt9*$^{-/-}$ littermates revealed acanthosis, hyperkeratosis, and occasional hypergranulosis within the footpads of *Krt9*-null mice (Figure 2a and Supplementary Figure S2 online). Compared to *Krt9*$^{+/+}$ and *Krt9*$^{+/-}$ littermates, the epidermis of *Krt9*$^{-/-}$ footpad regions was thicker and papillomatous. Within the stratum

granulosum of these mice, impaired keratinocyte flattening was observed, which coincided with the presence of larger, abnormally shaped, and nucleated keratinocytes (Figure 2a and Supplementary Figure S2 online). Importantly, these hyperkeratotic features were not present in the inter-footpad plantar epidermis of any of the animals studied (Figure 2b; and data not shown). Finally, Fontana–Masson staining revealed that melanin staining was specific to *Krt9*$^{-/-}$ fore-paw footpad sections (Supplementary Figure S3 online), indicating an increased presence of melanosomes.

In an attempt to quantify the differences in footpad and inter-footpad epidermal thickness between the *Krt9* genotypes, 10 independent measurements of these fore-paw tissues were taken and the average thickness across the footpad and inter-footpad regions calculated. When comparing the three geno-types, negligible differences were observed in the thickness of the inter-footpad regions. In contrast, although similar footpad thickness was recorded for *Krt9*$^{+/+}$ and *Krt9*$^{+/-}$ tissues, *Krt9*$^{-/-}$ footpads were ∼3 times thicker than their littermates (Figure 2b). The same trend was observed in a separate analysis of the hind-paws (data not shown), but the hyperkeratosis and acanthosis observed here were generally less severe than in the fore-paws (Supplementary Figure S2 online).

Ultrastructural analysis of keratotic phenotypes in *Krt9*$^{-/-}$ mice

Low magnification scanning electron microscopy was used to further examine the major fore-paw footpads of 8-week old *Krt9*$^{+/+}$, *Krt9*$^{+/-}$, and *Krt9*$^{-/-}$ littermates (Supplementary Figure S4 online). The major footpads of *Krt9*$^{+/+}$ and *Krt9*$^{+/-}$ mice were similar in size and were smooth. In contrast, *Krt9*$^{-/-}$ footpads were larger and had an uneven, rough surface with significant fissures (Supplementary Figure S4 online). These surface features were reminiscent of the epidermal thickening and fissuring observed in various human keratodermas caused by keratin gene mutations (Morais *et al.*, 2009). Transmission electron microscopy ultrastructural analysis comparing the footpad epidermis of *Krt9*$^{+/+}$ to *Krt9*$^{-/-}$ was carried out. This confirmed that loss of K9 results in acanthotic and hyperkeratotic fore-paw footpads, and revealed cytolysis-associated splits through the spinous layer (Figure 3a and Supplementary Figure S5 online). In addition, widespread pallor and a general lack of keratin intermediate filaments was observed in *Krt9*$^{-/-}$ spinous layer keratinocytes (Figure 3b). These findings suggest that the spinous layer may be the site of maximal weakness in *Krt9*$^{-/-}$ fore-paw footpads. Interestingly, despite a reduction in keratin filaments, no morphological differences were observed between the desmosomes of *Krt9*$^{+/+}$ and *Krt9*$^{-/-}$ mice (Figure 3c). This is consistent with observations made in *Krt5*-null, *Krt6a/b*-null, *Krt14*-null, and *Krt18*-null mice (Lloyd *et al.*, 1995; Magin *et al.*, 1998; Wong *et al.*, 2000; Peters *et al.*, 2001), as well as patients with *KRT14*-null mutations (Jonkman *et al.*, 1996; Chan *et al.*, 2000).

Proliferation and differentiation are disrupted in the absence of K9

The acanthotic and hyperkeratotic phenotypes observed in the *Krt9*$^{-/-}$ footpads prompted us to examine whether the
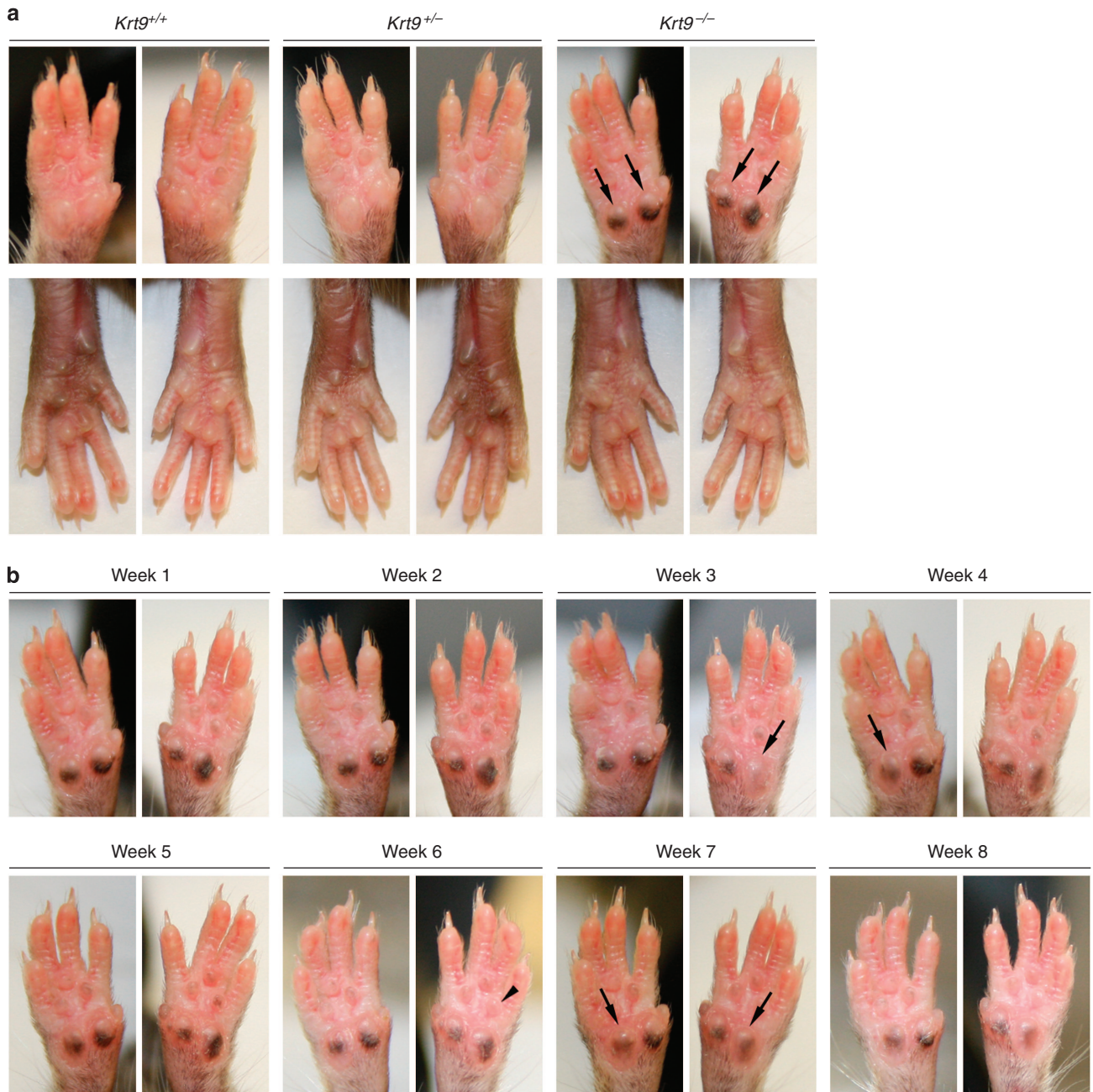
Figure 1. The stress-bearing footpads of fore-paws in keratin 9-deficient (Krt9$^{-/-}$) mice develop hyperpigmented calluses. The fore- and hind-paws of 8-week old Krt9$^{+/+}$, Krt9$^{+/-}$, and Krt9$^{-/-}$ littermates (n = 4 per genotype) were photographed weekly over an 8-week period. (**a**) Initial observation in week 1 revealed hyperpigmented calluses on the major stress-bearing fore-paw footpads of adult Krt9$^{-/-}$ mice (arrows). (**b**) In Krt9$^{-/-}$ mice, callus size and hyperpigmentation state grew and intensified, respectively, over a ~3-week period on the major footpads before sloughing off (arrows). Similar, but milder, calluses were also observed on the minor fore-paw footpads of Krt9$^{-/-}$ mice, which also appeared to cycle but at a slower rate (arrowhead).

expression and/or localization of proliferation and terminal differentiation markers were altered in response to loss of K9. Immunoperoxidase staining for the proliferation marker Ki-67 and the transcription factor p63, a key regulator of basal keratinocyte proliferation, differentiation, and survival (Candi *et al.*, 2008), revealed an increase in the number and staining intensity of Ki-67- and p63-positive cells, respectively, in the footpads of Krt9$^{-/-}$ mice (Figure 4). Quantification of the

number of Ki-67-positive basal keratinocytes revealed an increase in these cells in Krt9$^{-/-}$ tissues (83%) compared with Krt9$^{+/+}$ (60%) and Krt9$^{+/-}$ (58%) footpads (data not shown).

These findings and our observation that Krt9$^{-/-}$ granular keratinocytes failed to compact into a well-ordered granular layer, prompted us to investigate whether loss of K9 affected keratinocyte differentiation. This was achieved by examining
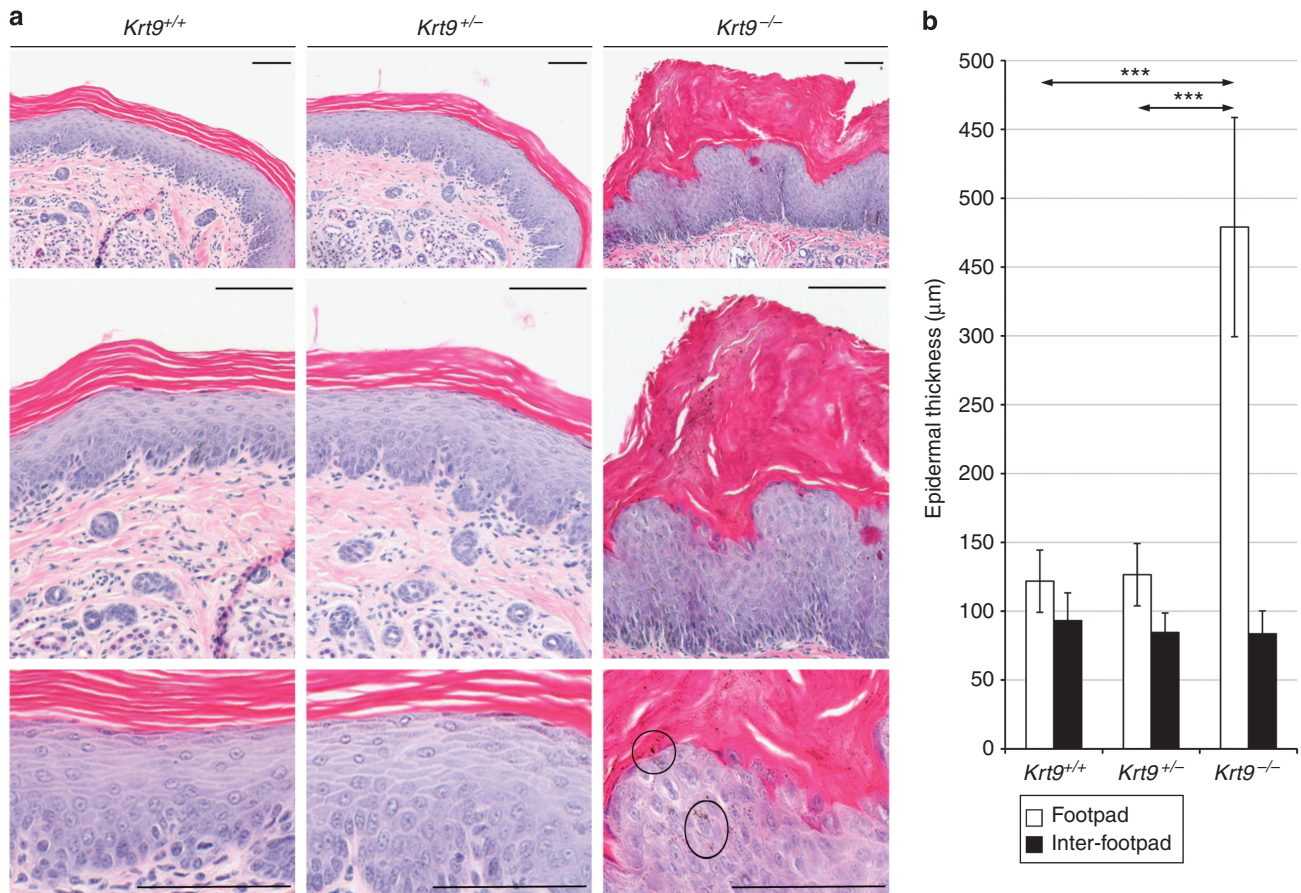
Figure 2. Localized keratotic phenotypes develop in adult keratin 9-deficient (Krt9$^{-/-}$) footpads. (**a**) Hematoxylin and eosin-stained cross-sections of formalin fixed, paraffin-embedded major fore-paw footpads of *Krt9$^{+/+}$*, *Krt9$^{+/-}$*, and *Krt9$^{-/-}$* littermates (*n* = 3 per genotype) revealed acanthosis, hyperkeratosis, and sporadic hypergranulosis in *Krt9$^{-/-}$* mice. Granular keratinocytes also failed to compact in these animals and dark pigment granules (circled) were observed in all strata. Scale bar = 100 μm. (**b**) Axiovision imaging software was used to measure the thickness of the footpad and inter-footpad epidermis in hematoxylin and eosin-stained fore-paw cross-sections from *Krt9$^{+/+}$*, *Krt9$^{+/-}$*, and *Krt9$^{-/-}$* animals. Graph depicts the mean thickness of each region calculated from 10 independent measurements taken over the length of a representative section from each genotype (*n* = 3) and the error bars represent SD. ***$P \leqslant 0.0001$.

the epidermal localization profiles of the stratum granulosum markers, loricrin and filaggrin (Candi *et al.*, 2005), in *Krt9$^{+/+}$*, *Krt9$^{+/-}$*, and *Krt9$^{-/-}$* littermates (Figure 4). Although both loricrin and filaggrin localized appropriately to the stratum granulosum of *Krt9$^{-/-}$* fore-paw footpads, a significant increase in loricrin staining intensity and retention within the stratum corneum was observed. In addition, compared with *Krt9$^{+/+}$* and *Krt9$^{+/-}$* sections, intermittent and disorganized filaggrin staining was observed in *Krt9$^{-/-}$* footpads. Collectively, these findings suggest that the localized acanthosis and hyperkeratosis phenotypes may be triggered by an increase in the proliferation state of basal keratinocytes and more rapid transition towards terminal differentiation, which ultimately impairs terminal differentiation and cornification.

Loss of K9 alters the expression patterns of a subset of palmoplantar keratins
Immunoperoxidase staining and western blotting were used to determine whether K9 ablation affected the levels and localization patterns of the other keratins expressed in the footpad

(Schweizer *et al.*, 1989; Swensson *et al.*, 1998). Importantly, due to the localized expression of K9 in the footpads and the footpad-restricted hyperkeratosis in K9-null mice we analyzed these regions separately from the inter-footpad tissues (Figure 5 and Supplementary Figure S6 online).

While the basal layer keratins, K5 and K14, were appropriately localized to the basal layer in *Krt9$^{+/+}$* and *Krt9$^{+/-}$* footpads, their localization patterns extended into the suprabasal epidermis, and as far up as the uppermost granular layer, in some regions in *Krt9$^{-/-}$* footpad tissues (Figure 5a). Semiquantitative western blotting for K14 demonstrated that the spatial localization changes did not affect its overall abundance (Figure 5b). Surprisingly, compared with *Krt9$^{+/+}$* tissues, we noted a 53% decrease in K5 protein levels only in *Krt9$^{-/-}$* footpads (Figure 5b and c, and Supplementary Figure S6 online). The levels and distribution of the suprabasal keratins, K1 and K10, did not change significantly in response to loss of K9 in neither the footpad (Figure 5a and b), nor the inter-footpad regions (Supplementary Figure S6 online). Finally, K2 staining revealed that
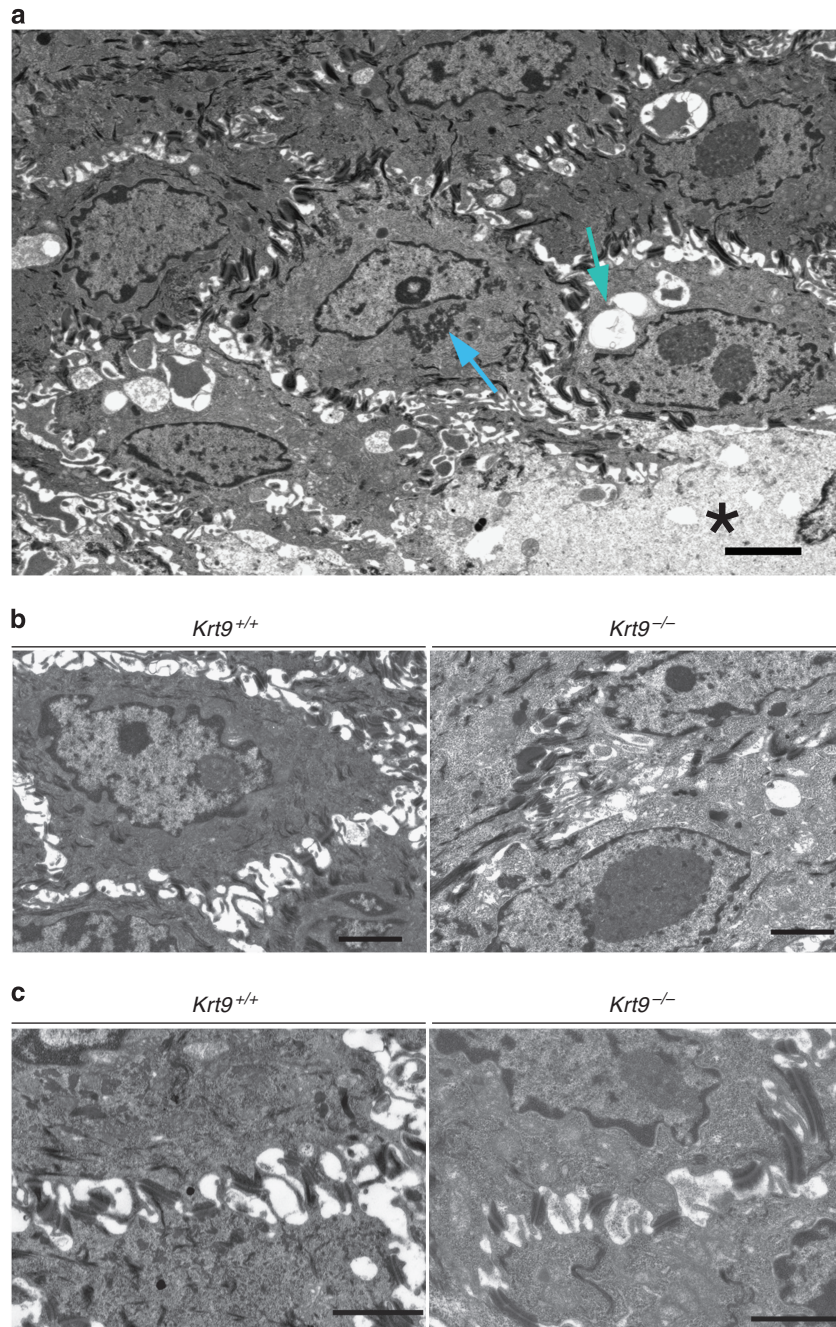
Figure 3. Ultrastructural analysis of keratin 9-deficient (Krt9$^{-/-}$) fore-paw footpads shows disrupted cytoskeletal integrity and keratin filament assembly. (**a**) Krt9$^{-/-}$ keratinocytes adjacent to the area of blistering (asterisk) show cytoplasmic disruption with evident cytolysis (green arrow), fewer keratin filaments and some filament, or keratin protein aggregation (blue arrow). Scale bar = 1 mm. (**b**) Compared with Krt9$^{+/+}$, loss of K9 in leads to relative pallor in Krt9$^{-/-}$ keratinocyte cytoplasm. Scale bar = 0.2 mm. (**c**) Despite loss of K9 (right panel), desmosome cell–cell junctions are similar in size and morphology to Krt9$^{+/+}$ desmosomes (left panel). Interestingly, fewer keratin filaments are seen in the adjacent cytoplasm in Krt9$^{-/-}$ fore-paw tissues. Both Krt9$^{+/+}$ and Krt9$^{-/-}$ desmosomes shown here are within the mid-spinous layer. Scale bar = 0.1 mm.

this keratin is specifically expressed at the borders of the glabrous footpad and within the inter-footpad regions of the plantar epidermis (Figure 5a and data not shown). In addition, semiquantitative western blotting demonstrated that the levels of K2 decreased by 60% in the fore-paw footpads in Krt9$^{-/-}$ animals compared with Krt9$^{+/+}$ and Krt9$^{+/-}$ mice (Figure 5b

and c). Similar reductions in K2 protein levels were also noted in Krt9$^{-/-}$ inter-footpad tissues (Supplementary Figure S6 online).

In addition to the palmoplantar keratins, we also determined how K9 ablation affected the expression of the stress-response and wound-healing keratins, K6 and K16
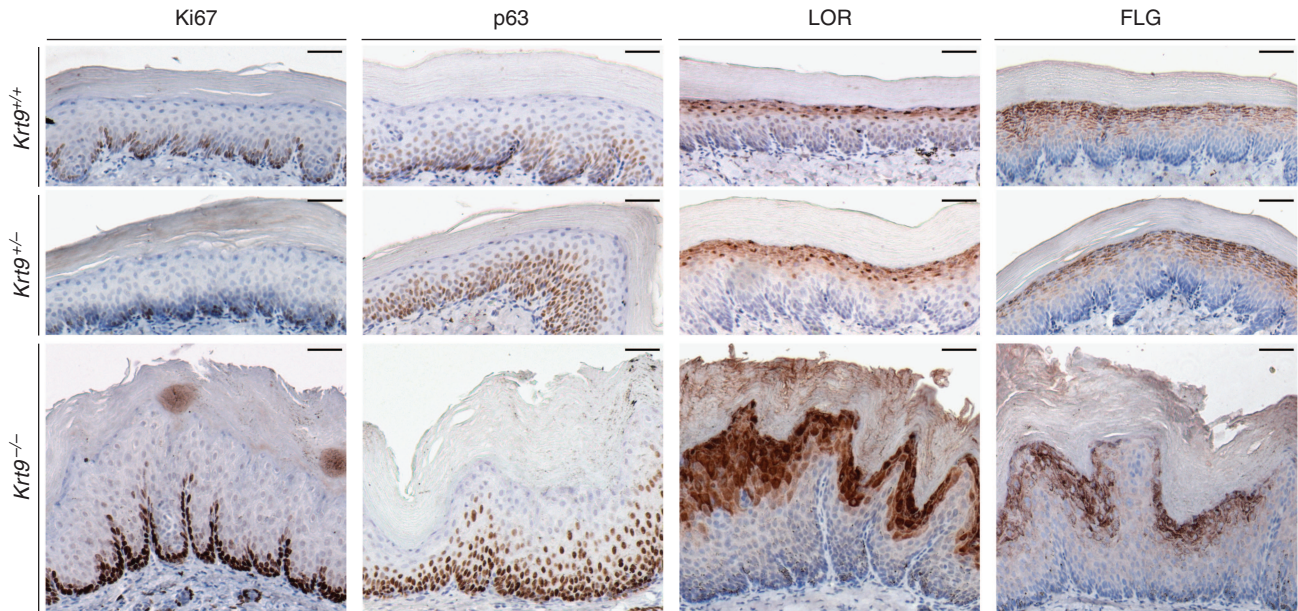
Figure 4. Hyperproliferation in adult keratin 9-deficient (Krt9$^{-/-}$) footpad epidermis. Immunoperoxidase staining of formalin fixed, paraffin-embedded fore-paw footpads from Krt9$^{+/+}$, Krt9$^{+/-}$, and Krt9$^{-/-}$ littermates ($n = 3$ per genotype) with α-Ki-67 (Ki67; MM1-L-CE), α-p63 (p63; SC8431), α-loricrin (LOR; AF62), and α-filaggrin (FLG; gift from Richard Presland, Seattle, WA) antibodies. Note the overall increase in Ki-67-positive basal layer keratinocytes, as well as increased Ki-67 and p63 staining intensities, in the Krt9$^{-/-}$ cross-sections relative to Krt9$^{+/+}$ and Krt9$^{+/-}$ samples. Although both FLG and LOR localized to the stratum granulosum in all genotypes, LOR staining in Krt9$^{-/-}$ cross-sections was stronger and extended into the stratum corneum. In addition, FLG appeared patchy and disorganized in Krt9$^{-/-}$ samples. Scale bar = 50 μm.

(Leigh *et al.*, 1995). Immunoperoxidase staining for K6 in Krt9$^{+/+}$, Krt9$^{+/-}$, and Krt9$^{-/-}$ littermates revealed that *Krt6* expression was specifically and exclusively induced in the suprabasal layers of Krt9$^{-/-}$ glabrous footpad tissues (Figure 5a). Moreover, K6 and K16 were only detectable by western blotting in Krt9$^{-/-}$ footpad lysates (Figure 5b). Quantification of Krt9$^{-/-}$ signals, relative to Krt9$^{+/+}$ and Krt9$^{+/-}$ signals, revealed ~15- and ~11-fold increases in K6 and K16 respective band intensities (Figure 5d). Surprisingly, increased K16 levels were also detected in Krt9$^{-/-}$ inter-footpad tissues despite the absence of hyperkeratosis in these areas (Supplementary Figure S6 online).

DISCUSSION

K9-null mice developed hyperpigmented calluses on the major stress-bearing footpads of the fore-paws, which were also sporadically visible on minor footpads of both the fore- and hind-paws. Histologically, these lesions showed prominent hyperkeratosis and acanthosis, which resulted in significant footpad epidermal thickening. Importantly, this well-circumscribed phenotype coincides with the footpad-restricted *Krt9* expression pattern observed here and reported previously (Schweizer *et al.*, 1989). These findings demonstrate that K9 is required for normal palmoplantar physiology, that its loss cannot be tolerated *in vivo* and begin to explain why K9 is evolutionarily conserved in mammals. Moreover, our data imply that K9 provides the critical mechanical reinforcement required for these weight-bearing tissues to withstand the continual load-bearing impact. This is supported by our observation that the most severe forms of the K9-null kera-

toderma phenotype develop on the major impact-dampening footpads of the main weight-bearing paws, the fore-paw, of the mice.

Melanin staining suggests that the hyperpigmentation phenotype, which accompanies Krt9$^{-/-}$ footpad hyperkeratosis and acanthosis, results, at least in part, from a marked increase in the number of melanosomes present in Krt9$^{-/-}$ fore-paw footpad tissues. As increased melanocyte infiltration at the dermal–epidermal interface and/or melanocyte proliferation could also contribute to this phenotype (Yamaguchi *et al.*, 2007), additional experiments are required to fully define the molecular cause of Krt9$^{-/-}$ fore-paw footpad hyperpigmentation. Moreover, ultrastructural analyses of the localized phenotype showed cytolysis-associated suprabasal splits with a significant reduction of keratin filaments. Compared with wild-type samples, alterations in the number and morphology of desmosomes in these regions were not observed in K9-null footpad tissues. Nevertheless, as fewer intermediate filaments are present in Krt9$^{-/-}$ tissues, additional studies defining the molecular composition and functional integrity of these Krt9$^{-/-}$ desmosomes are required. These studies will allow us to pin-point the molecular source of Krt9$^{-/-}$ footpad weakness and determine whether compromised desmosome function contributes to phenotype development.

The EPPK-like phenotype observed here was less severe than that recently reported in K16-null animals (Lessard and Coulombe, 2012). Krt16$^{-/-}$ mice develop an explicit palmoplantar keratoderma, similar to that seen in the human K16 subtype of pachyonychia congenita 16 (McLean *et al.*, 1995; McLean and Moore, 2011), which compromised animal
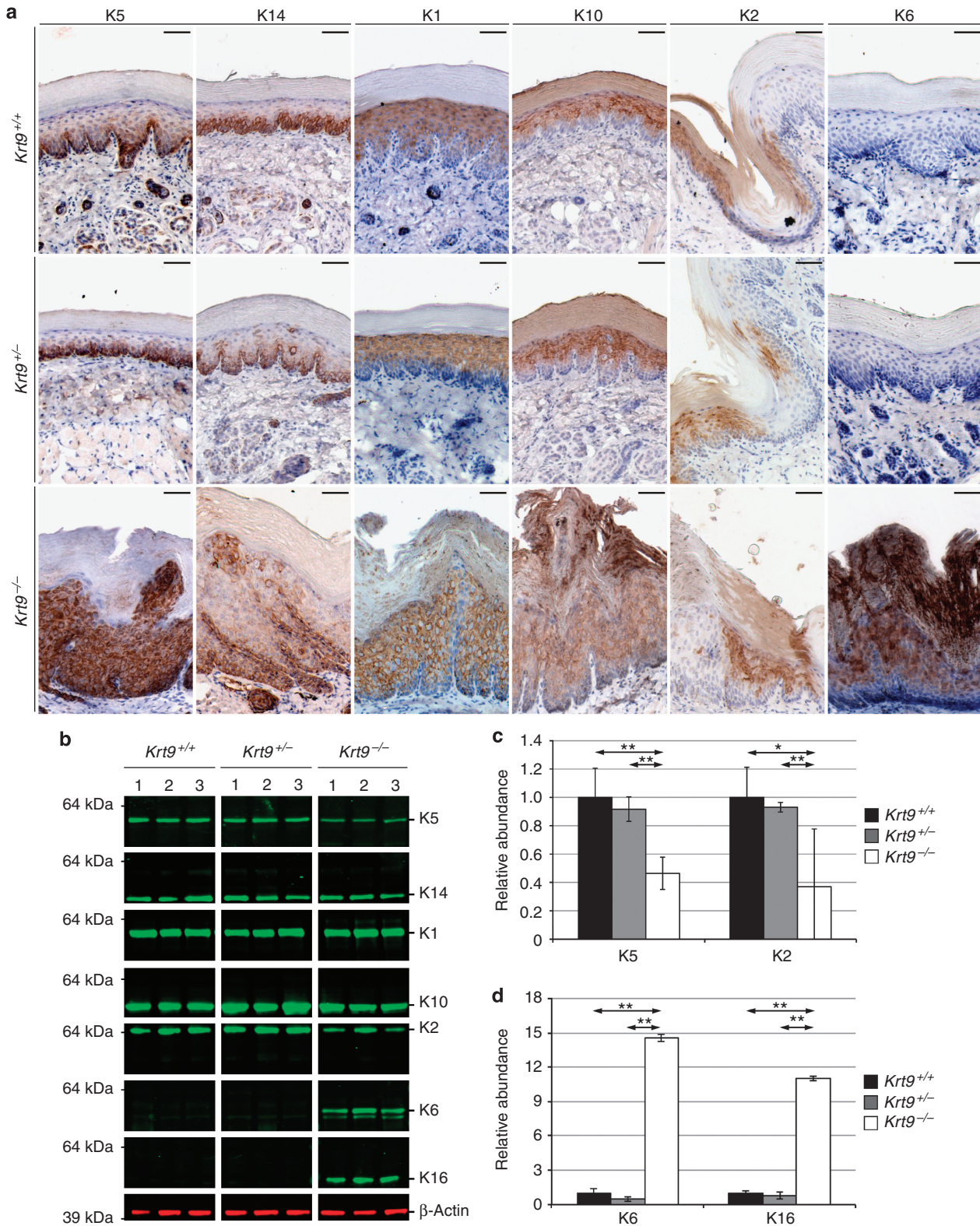
Figure 5. Keratin 9-deficient ($Krt9^{-/-}$)-knockout alters the expression patterns of a subset of palmoplantar keratins. (a) Immunoperoxidase staining of fore-paw footpads from $Krt9^{+/+}$, $Krt9^{+/-}$, and $Krt9^{-/-}$ littermates ($n=3$ per genotype) with α-K5, α-K14, α-K1, α-K10, α-K2, and α-K6. Note increased suprabasal staining of K5 and K14, and increased K6 staining in $Krt9^{-/-}$ cross-sections. Scale bar = 50 μm. (**b**) Immunoblotting of fore-paw footpad whole-tissue lysates $Krt9^{+/+}$, $Krt9^{+/-}$, and $Krt9^{-/-}$ littermates ($n=3$ per genotype) with α-K5, α-K14, α-K1, α-K10, α-K2, α-K6, α-K16, and α-β-actin (loading control; representative image shown) antibodies and differential fluorescence visualization. (**c, d**) Semiquantitative immunoblotting analyses of α-K5, α-K2, α-K6, and α-K16, relative to β-actin, were used to quantify protein abundance changes following loss of K9. Mean relative abundances ($n=3$) are shown, and error bars indicate signal intensity SD. *$P \leqslant 0.05$; **$P \leqslant 0.01$.

mobility and appeared painful. When comparing EPPK and pachyonychia congenita 16 with the recessive K9-null and K16-null palmoplantar keratodermas, respectively, it is interesting how closely the human and rodent disease severities and functional consequences mimic one another. Indeed, similar to what was observed in the K9-null and K16-null animals, the clinical features of EPPK are much milder and do not appear to affect the patient's quality of life as significantly as pachyonychia congenita 16, which can be extremely painful and severely debilitating for patients (McLean and Moore, 2011; Haines and Lane, 2012).

Further examination of the K9-null phenotype revealed an induction in the expression of the stress-activated keratins K6 and K16 (Leigh *et al.*, 1995) within the major footpads of the fore-paws. Surprisingly, we also found increased levels of K16 in seemingly unaffected inter-footpad epidermis where K9 is normally not expressed, suggesting that a trauma-induced paracrine signaling mechanism controls *Krt16* expression. Why K6 was not also induced here is unclear, but this may indicate that the K16 gene is more sensitive to this unknown paracrine effect. Perhaps nominal inter-footpad stress caused by K9-null footpad mechanical weakness triggers a sufficient response to induce K16, but not K6. Moreover, intensified footpad Ki-67 and p63 staining suggests that regional stress/weakness stimulates keratinocyte proliferation, which ultimately results in epidermal thickening. This process is somewhat analogous to what is observed in human dominant-negative keratin disorders, including EPPK, epidermolytic ichthyosis, or superficial epidermolytic ichthyosis (previously known as ichthyosis bullosa of Siemens; Oji *et al.*, 2010; McLean and Moore, 2011; Haines and Lane, 2012), where suprabasal mechanical fragility leads to overgrowth of the affected tissue. Terminal differentiation was also clearly disrupted in the footpad epidermis of K9-null mice. Changes in key epidermal barrier proteins, such as loricrin and filaggrin, were also noted. The highly abnormal, grossly thickened stratum corneum in $Krt9^{-/-}$ animals suggests that additional changes in corneocyte integrity, skin barrier proteins and lipid components may occur secondary to loss of K9.

In addition to the very apparent upregulation of stress-related keratins, a number of more subtle secondary effects on other keratins were observed in the footpads of K9-null mice. Due to the high degree of sequence homology shared by K10 and K9, and their overlapping suprabasal palmoplantar expression patterns (Reichelt *et al.*, 2001), it has long been postulated that K9 may also interact with K1 in the palmoplantar epidermis. If true, one might expect a similar decrease in K1 protein levels in the footpads of K9-null mice as observed following K10 ablation (Reichelt and Magin, 2002). As no change in the quantity or distribution of K1 was observed in $Krt9^{-/-}$ footpads, K9 may not interact with K1 here. Surprisingly, K5 protein levels decreased in $Krt9^{-/-}$ tissues suggesting that K5 may be the type II keratin-binding partner of K9 in the palmoplantar/footpad epidermis. Overall, the reduction in keratin protein levels was very subtle given the striking reduction in visible intermediate filaments by electron microscopy. This, and the presence of keratin protein aggregates in $Krt9^{-/-}$ spinous layer keratinocytes, suggests that the pool of soluble keratins increases in these tissues; presumably due to impaired keratin polymerization.

Further work is required to fully define the direct and indirect interactions and assembly preferences for the complex mixture of keratins found in footpad/palmoplantar epidermis. In the future, it will also be important to catalogue and understand how loss of a suprabasal keratin affects the stratum corneum and impedes terminal differentiation. Such experiments are essential when considering the potential implications therapeutic manipulation will have on keratin expression. Moreover, although the primary genetic basis of several keratin disorders is well understood, the secondary molecular mechanisms and signaling pathways involved in producing hyperkeratosis, regardless of the genetically determined mechanical insult (dominant mutation or ablation of various keratins), remain poorly understood. The availability of K9-null mice, which develop a form of hyperkeratosis similar to that seen in human keratinizing disorders, will facilitate future systems biology studies aimed at identifying candidate pathways and signaling molecules involved in this process. Indeed, identification of such common pathways, if they exist, could seed the development of a generic treatment for hyperkeratotic skin conditions.

It is clear that K9 is not completely dispensable in mice, therefore it is unlikely that siRNAs aimed at complete *KRT9* deletion in EPPK patients will be a therapeutically viable option. Importantly, this study has demonstrated that the palmoplantar epidermis develops normally in heterozygous K9-null mice and established that a single copy of *Krt9* is sufficient to maintain healthy skin *in vivo*. These results are of great significance as they indicate that the mutation-specific siRNA we recently developed for treating EPPK (Leslie Pedrioli *et al.*, 2012) are clinically viable and may, indeed, prove to be therapeutically beneficial for patients.

In conclusion, we have shown that K9 is required for mouse footpad epidermis mechanical integrity and correct terminal differentiation and, by implication, in the palmoplantar epidermis in humans. In addition to providing supportive data to justify our pursuit of mutation-specific RNA interference-based treatments for EPPK, this new mouse model is a valuable asset for future studies aimed at understanding the process of hyperkeratosis and potentially developing more generic treatments for hyperkeratotic skin conditions.

MATERIALS AND METHODS
Generation of $Krt9^{-/-}$ mice
All experiments involving mice followed the UK animal welfare act guidelines. K9-null mice were generated using *Krt9-null C57 Bl/6NTac* ES cells as described in the Supplementary Information online. F1 offspring were identified using Knock-Out Mouse Project repository genotyping protocols and all experiments were performed using age-matched littermates.

Histopathology and immunohistochemistry
The fore- and hind-paw footpad epidermis from 8-week-old gender-matched $Krt9^{+/+}$, $Krt9^{+/-}$, and $Krt9^{-/-}$ littermates ($n = 3$ per genotype) were dissected and fixed in neutral buffered formalin

(361387P, VWR International, Leicestershire, UK) for 48 h. Tissues were dehydrated, paraffin embedded, 7 μm sections cut, mounted on superfrost-plus slides (6310108, VWR International), and dried. For histopathological analyses, sections were deparaffinized and hematoxylin/eosin stained according to standard protocols. Epidermal thickness was measured using AxioVision Rel. 4.6 software (Zeiss, Cambridge, UK).

Immunohistochemical staining was performed as previously described (Leachman *et al.*, 2005) using the primary antibodies and the dilutions described in Supplementary Table S1 online. Antibody staining was visualized using anti-mouse or anti-rabbit EnVision+ system horseradish peroxidase-conjugated secondary antibodies and the liquid DAB+ substrate chromogen system (Dako, Cambridgeshire, UK). Fontana–Masson staining was carried as described in Manual of Histological Demonstration Techniques (Cook, 1974). All sections were counter-stained with hematoxylin. Images were acquired using an Axioskop microscope (12067, Zeiss), Axiocam 2 (24700, Zeiss), and AxioVision Rel. 4.6 software.

Immunoblotting

Footpad and inter-footpad epidermis of fore- and hind-paws were dissected from 8-week-old gender-matched $Krt9^{+/+}$, $Krt9^{+/-}$, and $Krt9^{-/-}$ littermates ($n=3$ per genotype) and snap-frozen in liquid nitrogen. Whole-tissue protein lysates were prepared via mortar and pestle grinding and reconstituted in $1\times$ denaturing NuPAGE LDS sample buffer (Life Technologies, Paisley, UK). Immunoblots were simultaneously probed with 1:2,000 rabbit anti-β-actin (loading control; ab8227, Abcam, Cambridge, UK) and the primary antibodies/dilutions listed in Supplementary Table S1 online. Blots were processed and visualized as previously described (Leslie Pedrioli *et al.*, 2012). Colored images were generated using Adobe Photoshop (Adobe Systems, San Jose, CA). Semiquantitative immunoblot analyses were performed using the GelEval 3.5 software (www. frogdance.dundee.ac.uk) as previously described (Leslie Pedrioli *et al.*, 2012).

Scanning electron and transmission electron microscopy

For scanning electron microscopy, whole fore- and hind-paws from 8-week-old gender-matched littermates were fixed in Peter's fixative (0.08 M sodium cacodylate [pH 7.4], 1% paraformaldehyde, and 1.25% glutaraldehyde) for 24 h. Secondary fixing was performed in either 1% OsO_4 for 1 h or 0.2% OsO_4 (aq) for 16–18 h. Specimens were rinsed in distilled water for 15 min, dehydrated through an ethanol gradient, and critical-point dried using a BAL-TEC CPD 030 (BAL-TEC, Schalksmühle, Germany). Samples were mounted on aluminum stubs, coated with 40 nm Au/Pd, and examined using a Philips XL30 ESEM (Philips, Eindhoven, The Netherlands) and XL Docu imaging software (Olympus Soft Imaging Solutions Munster, Germany).

For transmission electron microscopy, skin biopsy specimens were cut into small pieces (of $<1\,mm^3$) and fixed in half-strength Karnovsky fixative for 4 h at room temperature. After washing in 0.1 M sodium phosphate buffer (pH 7.4), samples were immersed in 1.3% aqueous osmium tetroxide (TAAB Laboratories, Berkshire, UK) for 2 h. Samples were then incubated in 2% uranyl acetate (Bio-Rad, Hercules, CA) and dehydrated in a graded ethanol series. Samples were embedded in epoxy resin via propylene oxide (TAAB Laboratories). Ultra-thin sections were stained with uranyl acetate and lead citrate and examined on a Philips CM10 transmission electron microscope (Philips).

SUPPLEMENTARY MATERIAL

Supplementary material is linked to the online version of the paper at http://www.nature.com/jid

REFERENCES

Candi E, Cipollone R, Rivetti di Val Cervo P *et al.* (2008) p63 in epithelial development. *Cell Mol Life Sci* 65:3126–33

Candi E, Schmidt R, Melino G (2005) The cornified envelope: a model of cell death in the skin. *Nat Rev Mol Cell Biol* 6:328–40

Chan YM, Ka-Leung Cheng D, Nga-Yin Cheung A *et al.* (2000) Female urethral adenocarcinoma arising from urethritis glandularis. *Gynecol Oncol* 79:511–4

Cook HC (1974) *Manual of Histological Demonstration Techniques,* Butterworths, London, 314p.

Coulombe PA, Tong X, Mazzalupo S *et al.* (2004) Great promises yet to be fulfilled: defining keratin intermediate filament function in vivo. *Eur J Cell Biol* 83:735–46

Haines RL, Lane EB (2012) Keratins and disease at a glance. *J Cell Sci* 125:3923–8

Jonkman MF, Heeres K, Pas HH *et al.* (1996) Effects of keratin 14 ablation on the clinical and cellular phenotype in a kindred with recessive epidermolysis bullosa simplex. *J Invest Dermatol* 107:764–9

Knapp AC, Franke WW, Heid H *et al.* (1986) Cytokeratin No. 9, an epidermal type I keratin characteristic of a special program of keratinocyte differentiation displaying body site specificity. *J Cell Biol* 103:657–67

Leachman SA, Kaspar RL, Fleckman P *et al.* (2005) Clinical and pathological features of pachyonychia congenita. *J Investig Dermatol Symp Proc* 10:3–17

Leigh IM, Navsaria H, Purkis PE *et al.* (1995) Keratins (K16 and K17) as markers of keratinocyte hyperproliferation in psoriasis in vivo and in vitro. *Br J Dermatol* 133:501–11

Leslie Pedrioli DM, Fu DJ, Gonzalez-Gonzalez E *et al.* (2012) Generic and personalized RNAi therapeutics for a dominant-negative epidermal fragility disorder. *J Invest Dermatol* 132:1627–35

Lessard JC, Coulombe PA (2012) Keratin 16-null mice develop palmoplantar keratoderma, a hallmark feature of pachyonychia congenita and related disorders. *J Invest Dermatol* 132:1384–91

Lloyd C, Yu QC, Cheng J *et al.* (1995) The basal keratin network of stratified squamous epithelia: defining K15 function in the absence of K14. *J Cell Biol* 129:1329–44

Lu H, Zimek A, Chen J *et al.* (2006) Keratin 5 knockout mice reveal plasticity of keratin expression in the corneal epithelium. *Eur J Cell Biol* 85:803–11

Magin TM, Schroder R, Leitgeb S *et al.* (1998) Lessons from keratin 18 knockout mice: formation of novel keratin filaments, secondary loss of keratin 7 and accumulation of liver-specific keratin 8-positive aggregates. *J Cell Biol* 140:1441–51

McLean WH, Irvine AD (2007) Disorders of keratinisation: from rare to common genetic diseases of skin and other epithelial tissues. *Ulster Med J* 76:72–82

McLean WH, Rugg EL, Lunny DP *et al.* (1995) Keratin 16 and keratin 17 mutations cause pachyonychia congenita. *Nat Genet* 9:273–8

McLean WHI, Moore CBT (2011) Keratin disorders—from gene to therapy. *Hum Mol Genet* 20:R189–97

Morais P, Mota A, Baudrier T *et al.* (2009) Epidermolytic hyperkeratosis with palmoplantar keratoderma in a patient with KRT10 mutation. *Eur J Dermatol* 19:333–6

Oji V, Tadini G, Akiyama M *et al.* (2010) Revised nomenclature and classification of inherited ichthyoses: results of the First Ichthyosis Consensus Conference in Soreze 2009. *J Am Acad Dermatol* 63: 607–41

Omary MB, Coulombe PA, McLean WHI (2004) Intermediate filament proteins and their associated diseases. *New Eng J Med* 351:2087–100

Peters B, Kirfel J, Bussow H *et al.* (2001) Complete cytolysis and neonatal lethality in keratin 5 knockout mice reveal its fundamental role in skin integrity and in epidermolysis bullosa simplex. *Mol Biol Cell* 12:1775–89

Porter RM, Lane EB (2003) Phenotypes, genotypes and their contribution to understanding keratin function. *Trends Genet* 19:278–85

Reichelt J, Bussow H, Grund C *et al.* (2001) Formation of a normal epidermis supported by increased stability of keratins 5 and 14 in keratin 10 null mice. *Mol Biol Cell* 12:1557–68

Reichelt J, Magin TM (2002) Hyperproliferation, induction of c-Myc and 14-3-3sigma, but no cell fragility in keratin-10-null mice. *J Cell Sci* 115:2639–50

Schweizer J, Baust I, Winter H (1989) Identification of murine type I keratin 9 (73 kDa) and its immunolocalization in neonatal and adult mouse foot sole epidermis. *Exp Cell Res* 184:193–206

Smith F (2003) The molecular genetics of keratin disorders. *Am J Clin Dermatol* 4:347–64

Swensson O, Langbein L, McMillan JR *et al.* (1998) Specialized keratin expression pattern in human ridged skin as an adaptation to high physical stress. *Br J Dermatol* 139:767–75

Wong P, Colucci-Guyon E, Takahashi K *et al.* (2000) Introducing a null mutation in the mouse K6alpha and K6beta genes reveals their essential structural role in the oral mucosa. *J Cell Biol* 150:921–8

Yamaguchi Y, Brenner M, Hearing VJ (2007) The regulation of skin pigmentation. *J Biol Chem* 282:27557–61